



# The shared genetic architecture between schizophrenia and common peripheral organ imaging phenotypes

Yingying Xie<sup>1,2,6</sup>, Jiaojiao Du<sup>3,6</sup>, Zhen Zhao<sup>3</sup>, Jie Sun<sup>3</sup>, Ningnannan Zhang<sup>3</sup>, Zhang Zhang<sup>3</sup>, Feng Liu<sup>3</sup> and Dairong Cao<sup>1,2,4,5</sup>

Schizophrenia (SCZ) is a complex neuropsychiatric disorder that profoundly disrupts daily life. Beyond its well-documented effects on the brain, SCZ is also associated with peripheral organ dysfunction, yet the underlying shared genetic mechanisms remain unclear. In this study, leveraging large-scale genome-wide association study (GWAS) data, we investigated the genetic architecture shared between SCZ and 47 common imaging phenotypes spanning three major peripheral organs: 28 cardiac magnetic resonance (CMR) phenotypes, eight skeletal dual-energy X-ray absorptiometry (DXA) phenotypes, and 11 abdominal magnetic resonance imaging (MRI) phenotypes. We identified seven significant causal associations between SCZ and peripheral organ imaging phenotypes, alongside 99 unique loci through local genetic correlation analysis. Additionally, we pinpointed 437 independent pleiotropic SNPs between SCZ and CMR phenotypes, 257 for skeletal DXA phenotypes, and 230 for abdominal MRI phenotypes. The shared genes were significantly enriched in synapse-related biological processes, underscoring their vital role in SCZ across various peripheral organ systems. Furthermore, we characterized the spatiotemporal expression patterns of shared genes in the brain across different peripheral imaging phenotype groups and identified drug-gene interactions, highlighting potential therapeutic targets for SCZ-related peripheral dysfunction. Our findings underscore the systemic nature of SCZ, emphasizing the need to integrate psychiatric and systemic health perspectives in its management. By revealing novel genetic links and potential therapeutic targets, this study provides valuable insights into SCZ's multifaceted impact beyond the brain.

*Schizophrenia* (2025)11:122; <https://doi.org/10.1038/s41537-025-00670-6>

## INTRODUCTION

Schizophrenia (SCZ) is a complex and devastating psychiatric disorder characterized by several profound disruptions<sup>1</sup>. Despite extensive research into its psychiatric symptoms and brain impairments, SCZ is also increasingly recognized to involve damage to multiple peripheral organs. For example, SCZ patients exhibit cardiological structural and functional alterations<sup>2,3</sup>. SCZ patients (especially females) commonly present with decreased bone mineral density and impaired bone quality<sup>4,5</sup>. Besides, SCZ correlates with a high prevalence of non-alcoholic fatty liver disease, liver function abnormalities, iron metabolism dysregulation, and visceral adiposity, with these changes strongly associating with increased metabolic syndrome risk influenced by both antipsychotics and nutritional factors<sup>6–8</sup>. These systemic manifestations can complicate the clinical management of SCZ, underscoring the importance of accounting for both psychiatric and physiological aspects of the disorder<sup>9</sup>. Nevertheless, despite these clinical observations, the genetic and molecular mechanisms underlying the comorbidity between SCZ and peripheral organ dysfunctions remain largely unexplored.

The genetic basis of SCZ is well-documented with a high genetic heritability<sup>10,11</sup>. Genome-wide association studies (GWAS) have significantly enhanced the ability to identify the genetic architecture of complex diseases and traits, including SCZ and imaging phenotypes<sup>12–15</sup>. While traditional GWASs have been instrumental in identifying genetic variants associated with SCZ and various organ group-specific imaging phenotypes<sup>12–15</sup>, these methods alone may not fully capture the complex interplay

between SCZ and peripheral organ dysfunctions. To address this limitation, it is crucial to incorporate advanced genetic analysis methods that can provide a more nuanced understanding of shared genetic architecture<sup>16–18</sup>. For example, Mendelian randomization (MR) is a robust methodology employed to evaluate the potential causal relationships between distinct phenotypes<sup>19–22</sup>; Local analysis of [co]variance association (LAVA) is a statistical method used to investigate how groups of nearby genetic variants collectively contribute to the variability of a trait or disorder<sup>23</sup>, and the pleiotropic analysis under composite null hypothesis (PLACO) methodology is tailored to detect pleiotropic SNPs, which offers enhanced power in testing pleiotropy while maintaining flexibility and statistical robustness<sup>24</sup>.

Understanding how shared genetic factors contribute to both SCZ and its systemic effects could offer new perspectives on the pathophysiology of the disorder and highlight potential targets for intervention. By identifying these genetic pathways, we can pinpoint critical molecular targets, which could lead to more effective, holistic treatments that address both the neurological and systemic manifestations of SCZ, ultimately improving patient outcomes. In addition, identifying when and where shared genetic factors are expressed during development or adulthood can reveal the molecular processes underlying SCZ and its impact on peripheral organs. Furthermore, drug-gene interaction analyses hold promise for repurposing existing drugs or creating new treatments that target both psychiatric symptoms and systemic complications of SCZ.

<sup>1</sup>Department of Radiology, The First Affiliated Hospital of Fujian Medical University, Fuzhou, Fujian, China. <sup>2</sup>Department of Radiology, National Regional Medical Center, Binhai Campus of the First Affiliated Hospital, Fujian Medical University, Fuzhou, Fujian, China. <sup>3</sup>Department of Radiology, Tianjin Key Laboratory of Functional Imaging & Tianjin Institute of Radiology, Tianjin Medical University General Hospital, Tianjin, China. <sup>4</sup>Fujian Key Laboratory of Precision Medicine for Cancer, the First Affiliated Hospital, Fujian Medical University, Fuzhou, Fujian, China. <sup>5</sup>Key Laboratory of Radiation Biology of Fujian Higher Education Institutions, the First Affiliated Hospital, Fujian Medical University, Fuzhou, Fujian, China. <sup>6</sup>These authors contributed equally: Yingying Xie, Jiaojiao Du. ✉email: [fengliu@tmu.edu.cn](mailto:fengliu@tmu.edu.cn); [dairongcao@fjmu.edu.cn](mailto:dairongcao@fjmu.edu.cn)

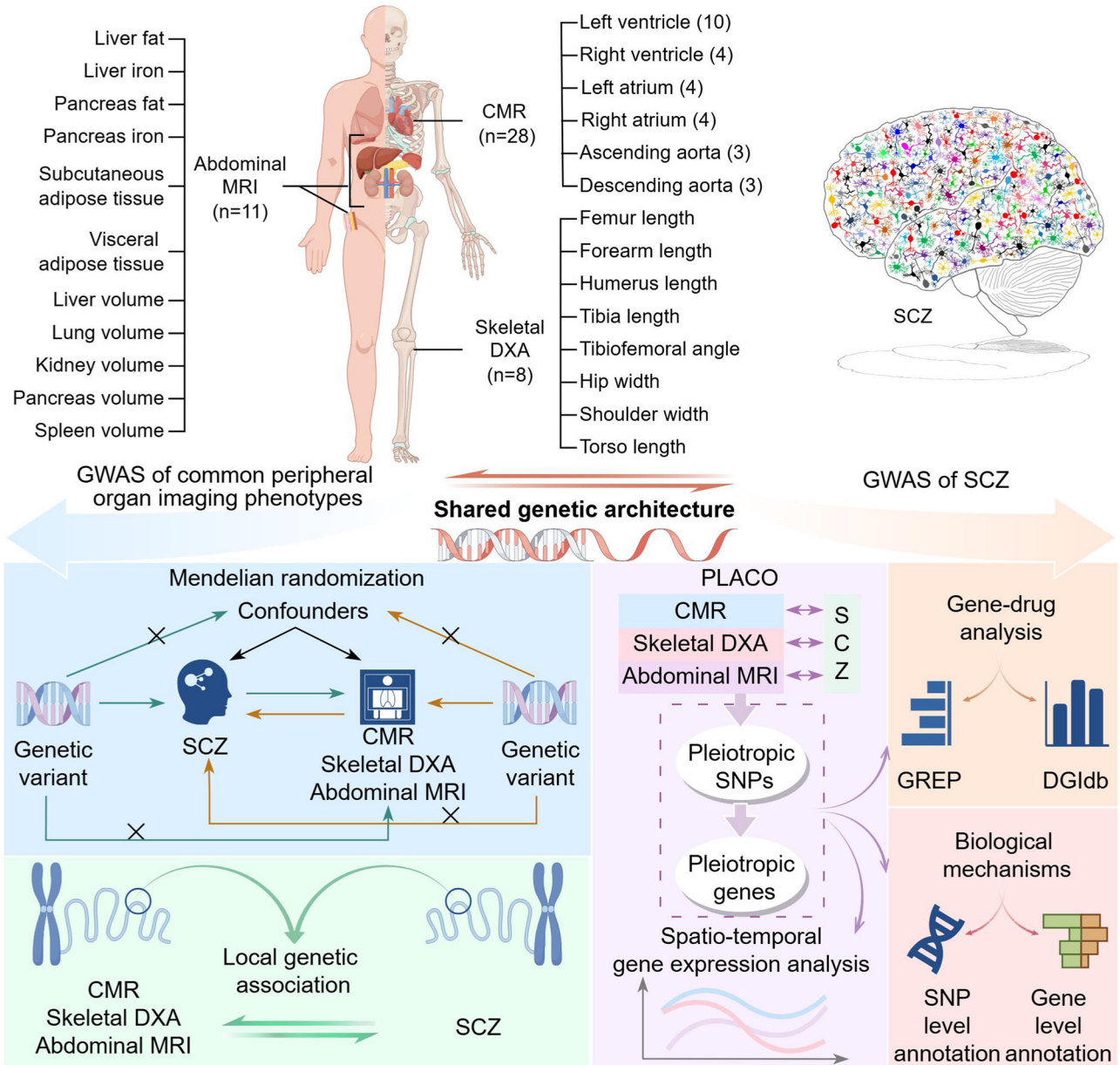


**Fig. 1 The flowchart of the study design.** By using the GWAS summary datasets of SCZ and 47 peripheral organ imaging phenotypes (28 from cardiac magnetic resonance, eight from skeletal dual-energy X-ray absorptiometry, and 11 from abdominal magnetic resonance imaging), we conducted Mendelian randomization and local genetic correlations between SCZ and each of the imaging phenotypes. The pleiotropic SNPs between SCZ and each of the peripheral organ imaging phenotypes were identified using PLACO, followed by functional annotations for derived pleiotropic SNPs and genes. Besides, distinct spatio-temporal gene expression patterns were uncovered based on the derived shared genes. Finally, drug category enrichment and gene-drug interactions were performed to enhance the clinical therapy. CMR cardiac magnetic resonance, DXA dual-energy X-ray absorptiometry, GWAS genome-wide association study, MRI magnetic resonance imaging, PLACO pleiotropic analysis under composite null hypothesis, SCZ schizophrenia, SNP single nucleotide polymorphisms.

In this study, we aim to explore the shared genetic architecture between SCZ and common peripheral organ imaging phenotypes. GWAS summary datasets of SCZ and 47 peripheral organ imaging phenotypes from European (EUR) populations were used. The common peripheral organ imaging phenotypes included 28 imaging phenotypes from cardiac magnetic resonance (CMR), eight imaging phenotypes from skeletal dual-energy X-ray absorptiometry (DXA), and 11 imaging phenotypes from abdominal magnetic resonance imaging (MRI). MR analyses were performed to explore the causal associations between SCZ and each of the imaging phenotypes, and LAVA analyses were conducted to identify the local

genetic correlations. Besides, pleiotropic SNPs were identified by PLACO, and critical biological processes were determined. Based on the derived shared genes across different organ imaging phenotypes, the spatio-temporal expression patterns of those genes in the brain were clarified. Finally, the potential therapeutic agents with clinical significance and therapeutic targets were investigated. The flowchart of the study design is shown in Fig. 1. These findings may contribute to a deeper understanding of the genetic and physiological interplay between SCZ and peripheral organ involvement, ultimately paving the way for integrated approaches to managing and treating this complex disorder.

## METHODS

### Genome-wide association study (GWAS) datasets

The European (EUR) GWAS summary dataset for schizophrenia (SCZ) was obtained from the Psychiatric Genomics Consortium (PGC)<sup>14</sup>, comprising 53,386 cases and 77,258 controls. A total of 47 EUR GWAS summary datasets of common peripheral organ imaging phenotypes were analyzed, comprising 28 cardiac magnetic resonance (CMR) phenotypes<sup>15</sup>, eight skeletal dual-energy X-ray absorptiometry (DXA) phenotypes<sup>12</sup>, and 11 abdominal magnetic resonance imaging (MRI) phenotypes<sup>13</sup>. The 28 CMR phenotypes from 31,875 individuals can be grouped into six categories, including the ascending aorta (AAo), descending aorta (DAo), the left ventricle (LV), right ventricle (RV), left atrium (LA), and right atrium (RA). The eight skeletal DXA phenotypes, comprising tibiofemoral angle, long bone lengths, hip width, and shoulder width, were derived from 31,221 full-body DXA images. All skeletal measurements were adjusted to account for individual height. The 11 abdominal MRI phenotypes include the volume of the lung, liver, kidney, spleen, and pancreas, as well as measurements of liver fat, liver iron, pancreas fat, pancreas iron, subcutaneous adipose tissue, and visceral adipose tissue. The detailed information of these GWAS datasets is shown in Supplementary Table 1.

### Mendelian randomization analysis

Mendelian randomization (MR) analyses were employed using the TwoSampleMR package (<https://mrcieu.github.io/TwoSampleMR/>)<sup>25</sup> to investigate the bidirectional genetic causal relationships between SCZ and each of the 47 imaging phenotypes. The instrumental variables were initially defined as SNPs with a significance level of  $P < 5 \times 10^{-8}$  in the exposure GWAS dataset. We applied linkage disequilibrium (LD) clumping with 500 kb and an  $r^2$  threshold of 0.2 with the 1000 Genomes European ancestry data as a reference panel (EUR-LD references), and palindromic SNPs were discarded. The MR Steiger directionality test<sup>26</sup> was employed to examine whether exposure was directionally causal for the outcome, and SNPs that did not meet were excluded. In cases where the outcome does not have a corresponding IVs, proxy SNPs were selected based on LD with an  $r^2$  greater than 0.8. We did not conduct MR analysis when the number of instrumental variables was fewer than five, as a limited number of instruments can reduce the robustness and reliability of the causal estimates. For sensitivity analysis, the intercept of the MR-Egger method was used to detect the directional pleiotropy, and the heterogeneity Q test was performed to evaluate the heterogeneity<sup>27,28</sup>.

We used the Inverse Variance Weighted (IVW)<sup>29</sup> method as the main analysis, and the significance threshold was defined as  $P < 5.32 \times 10^{-4}$ , which was Bonferroni corrected for 47 phenotypes and two directions. Additionally, we performed the Weighted median<sup>30</sup> and MR-Egger to validate the robustness of IVW estimates. When a significant estimate provided by IVW had the same effect direction as those provided by the other two methods, it was considered a reliable significant estimate.

### Local genetic correlation analysis

Local analysis of [co]variant association (LAVA, <https://github.com/josefin-werme/LAVA>)<sup>23</sup> was employed to conduct localized genetic associations between SCZ and the 47 imaging phenotypes. LAVA is capable of analyzing the standard bivariate local  $r_g$  between two phenotypes (binary as well as continuous)<sup>23</sup>. Given that the detection of valid and interpretable local genetic correlations necessitates the presence of adequate local genetic signals, univariate tests within the LAVA approach function as a preliminary filtering step for subsequent bivariate local genetic correlation analyses. The pre-defined 2495 loci were included, and the 1000 Genomes European ancestry data (GRCh37/hg19) was

utilized for the estimation of LD. Following this filtering process, bivariate local genetic correlation analyses were exclusively conducted for pairs of SCZ and each of the imaging phenotypes that exhibited a nominally significant univariate local genetic signal ( $P < 0.05$ ). We used FDR Benjamini–Hochberg (FDR-BH) significance level with FDR  $q < 0.05$  to assess the significance of bivariate genetic correlations, adjusting  $P$  for multiple tests.

### Identification of pleiotropic SNPs

To identify pleiotropic SNPs that are shared by SCZ and each of the imaging phenotypes, several processing steps were performed, including (1) excluding SNPs regions with complex LD structures (chr 6: 25,119,106–33,854,733 and chr 8: 7,242,715–12,483,982); (2) harmonizing the same effect allele across the study; (3) removing SNPs with squared Z-scores ( $Z^2 > 80$ ). We used the pleiotropic analysis under a composite null hypothesis (PLACO, <https://github.com/RayDebashree/PLACO>) to identify pleiotropic SNPs<sup>24</sup>. PLACO detects pleiotropic associations by considering a composite null hypothesis, which is divided into three sub-null hypotheses: (1)  $H_{00}$ : the SNP is not associated with either of the two phenotypes. (2)  $H_{10}$ : the SNP is associated with the phenotype<sub>1</sub> but not the phenotype<sub>2</sub>. (3)  $H_{01}$ : the SNP is not associated with the phenotype<sub>1</sub> but the phenotype<sub>2</sub>. The alternative hypothesis ( $H_{11}$ ) is that the SNP is related to both phenotypes, corresponding to pleiotropic association. In accordance with a previous study<sup>31</sup>, SNPs with  $P_{PLACO} < 1 \times 10^{-6}$  were declared as suggestive significant pleiotropic genetic signatures. Based on the derived pleiotropic SNPs, the independent pleiotropic SNPs were defined by LD clumping with 250 kb and an  $r^2$  threshold of 0.1 in EUR-LD references.

### Functional annotations for pleiotropic SNPs and genes

FUMA (<https://fuma.ctglab.nl/>)<sup>32</sup> was used to annotate the pleiotropic SNPs. Combined Annotation Dependent Depletion (CADD) score is a widely used tool that predicts the deleteriousness of SNPs for protein structure and function<sup>33</sup>. Higher CADD scores generally indicate potentially higher disease potential, with a threshold of 12.37. RegulomeDB (RDB) classifies SNPs according to the available evidence of regulatory functions<sup>34</sup>. Lower RDB scores indicate that SNPs are most likely affecting regulatory elements. The minChrState provides predictions of SNPs' transcriptional and regulatory effects in different chromatin states<sup>35</sup>. The predictions range from 1 to 15, and 1 to 7 predictions indicate an open chromatin state. ToppGene (<http://toppgene.cchmc.org>)<sup>36</sup> was used to conduct gene functional annotations for the nearest genes of the pleiotropic SNPs. The FDR Benjamini–Hochberg (FDR-BH) significance level with FDR  $q < 0.05$  was used for multiple comparison correction.

### Phenotype-wide association analyses with cognition

We performed phenotype-wide association analyses with eight cognitive phenotypes consistent with a previous study<sup>37</sup> based on the pleiotropic SNPs shared between SCZ and CMR phenotypes, skeletal DXA phenotypes, and abdominal MRI phenotypes, respectively (Supplementary Table 2). We defined a SNP as phenotype-wide significant if it reached genome-wide significance ( $P < 5 \times 10^{-8}$ ) in the GWAS of any of the eight cognitive phenotypes.

### Cell-type enrichment analysis

The cell-type-specific enrichment analysis was conducted using Web-based Cell-type-Specific Enrichment Analysis (WebCSEA, <https://bioinfo.uth.edu/webcsea/>)<sup>38</sup>, a bioinformatics platform designed to identify cell-type-enriched gene expression signatures from transcriptomic datasets. Genes shared between SCZ and imaging phenotypes were subjected to cell-type enrichment profiling.

### Spatio-temporal gene expression trajectory analysis

A spatio-temporal analysis of brain gene expression was conducted to investigate how the genes shared between SCZ and each of the peripheral organ imaging phenotypes are expressed at different stages of development. This approach may shed light on the potential roles these genes may play in the development of SCZ and potential peripheral organ changes. Here, we used the mRNA-seq data from PsychENCODE<sup>39,40</sup>, which included 607 tissue samples from 41 postmortem brains (18 females and 23 males) spanning 8 post-conception weeks (PCW) to 40 years of age (postnatal years, PY). The gene expression patterns were examined across nine developmental windows: 8–9 PCW, 12–13 PCW, 16–17 PCW, 19–22 PCW, 35 PCW to 4 months, 0.5–2.6 PY, 2.8–10.7 PY, 13–19 PY, and 21–40 PY<sup>39</sup>. Expression levels in RPKM (reads per kilobase of exon model per million mapped reads) were log<sub>2</sub>-transformed and normalized to the mean expression level for each sample<sup>39</sup>. For shared genes between SCZ and each group of the peripheral organ imaging phenotypes (CMR phenotypes, skeletal DXA phenotypes, and abdominal MRI phenotypes), averaged expression values were calculated, and smoothed LOESS curves were generated to illustrate the gene expression trajectories over time.

### Drug-target enrichment analysis and drug-gene interactions

The Genome for REPositioning Drugs (GREP, <https://github.com/saorisakaue/GREP>)<sup>41</sup> provides comprehensive data on 22,300 drugs and 2029 targets, sourced from DrugBank<sup>42</sup> and Therapeutic Target Database<sup>43</sup>. These drugs were further classified using the Anatomical Therapeutic Chemical (ATC) Classification System of the World Health Organization (WHO). Fisher's Exact Test was employed to determine whether the input gene sets were enriched in specific clinical indication categories, aiding in identifying potential treatments for diseases or conditions<sup>41</sup>. Furthermore, we used the drug-gene interaction database (DGIdb, <https://www.dgidborg>), a comprehensive resource cataloging drug-gene interactions, to gain insights into potential therapeutic targets and interactions<sup>44</sup>. It compiles data from public resources and uses sophisticated algorithms to infer potential interactions between drugs and genes. By examining the interaction types and interaction group scores, we were able to prioritize potential drug candidates that may have therapeutic potential for SCZ and peripheral organ imaging phenotypes.

## RESULTS

### The causal associations between SCZ and peripheral organ imaging phenotypes

Mendelian randomization analyses were performed to identify the bidirectional causal effects between SCZ and each of the peripheral organ imaging phenotypes by using the TwoSampleMR package (<https://mrcieu.github.io/TwoSampleMR/>)<sup>25</sup>. The Inverse Variance Weighted (IVW)<sup>29</sup> method was used as the main analysis, and the Weighted median<sup>30</sup> and MR-Egger were used to validate the robustness of IVW estimates. Results were deemed statistically significant after adjusting for multiple comparisons using the Bonferroni threshold ( $P < 5.32 \times 10^{-4}$ , corrected for 47 phenotypes and two directions).

Four significant positive causal effects for SCZ on peripheral organ imaging phenotypes were identified (SCZ→peripheral organ imaging phenotypes), including global myocardial-wall thickness at end-diastole (WT global;  $BETA_{IVW} = 0.024$ ,  $SE_{IVW} = 0.006$ ,  $P_{IVW} = 1.19 \times 10^{-4}$ , Fig. 2a), ascending aorta minimum area (AAo min area;  $BETA_{IVW} = 0.048$ ,  $SE_{IVW} = 0.010$ ,  $P_{IVW} = 8.93 \times 10^{-7}$ , Fig. 2b), left ventricular myocardial mass (LVM;  $BETA_{IVW} = 0.023$ ,  $SE_{IVW} = 0.005$ ,  $P_{IVW} = 2.09 \times 10^{-5}$ , Supplementary Fig. 1a), and ascending aorta maximum area (AAo max area;  $BETA_{IVW} = 0.048$ ,  $SE_{IVW} = 0.010$ ,

$P_{IVW} = 6.52 \times 10^{-7}$ , Supplementary Fig. 1b). Besides, we revealed negative causal effects for SCZ on the torso length ( $BETA_{IVW} = -0.001$ ,  $SE_{IVW} = 0.0002$ ,  $P_{IVW} = 3.64 \times 10^{-7}$ , Fig. 2c), pancreas volume ( $BETA_{IVW} = -0.045$ ,  $SE_{IVW} = 0.009$ ,  $P_{IVW} = 1.68 \times 10^{-7}$ , Fig. 2d), and subcutaneous adipose tissue measurement ( $BETA_{IVW} = -0.043$ ,  $SE_{IVW} = 0.009$ ,  $P_{IVW} = 6.88 \times 10^{-7}$ , Supplementary Fig. 1c). However, we did not observe any significant results when SCZ was treated as the outcome. The detailed results are shown in Supplementary Table 3.

### Local genetic correlations between SCZ and peripheral organ imaging phenotypes

To explore the genomic loci exhibiting pronounced genetic correlations between SCZ and peripheral organ imaging phenotypes, we estimated regional genetic correlations utilizing local analysis of [co]variant association (LAVA, <https://github.com/josefin-werme/LAVA>)<sup>23</sup>. Among the pre-defined 2495 loci (Supplementary Table 4), we first identified those exhibiting nominally significant local heritability ( $P < 0.05$ ). Subsequently, bivariate local genetic correlation analyses were conducted for these loci. At the FDR Benjamini–Hochberg (FDR-BH) significance level with FDR  $q < 0.05$ , the LAVA analysis uncovered 53 unique loci with a significant local genetic correlation between SCZ and CMR phenotypes, 18 unique loci for skeletal DXA phenotypes, and 30 unique loci for abdominal MRI phenotypes (Supplementary Fig. 2 and Supplementary Tables 5–7). For example, the linkage disequilibrium (LD) block 1945 (chr13: 107,037,865–108,521,978) was significantly associated with the maximum ( $r_g = 0.678$ , FDR  $q = 5.44 \times 10^{-3}$ ) and minimum ( $r_g = 0.644$ , FDR  $q = 1.06 \times 10^{-2}$ ) areas of the descending aorta and SCZ; both LD block 457 (chr3: 36,840,137–38,729,767;  $r_g = 0.874$ , FDR  $q = 2.04 \times 10^{-3}$ ) and LD block 692 (chr4: 102,544,804–104,384,534;  $r_g = -0.765$ , FDR  $q = 8.02 \times 10^{-9}$ ) were associated with femur length and SCZ; LD block 1500 (chr10: 12,581,572–13,208,061) was associated with kidney volume and SCZ ( $r_g = -1.000$ , FDR  $q = 9.84 \times 10^{-3}$ ).

### Pleiotropic SNPs shared by SCZ and peripheral organ imaging phenotypes

Pleiotropic analysis under composite null hypothesis (PLACO, <https://github.com/RayDebashree/PLACO>)<sup>24</sup> was used to identify pleiotropic SNPs between SCZ and each of the peripheral organ imaging phenotypes. In accordance with previous studies<sup>31</sup>, SNPs with  $P_{PLACO} < 1 \times 10^{-6}$  were identified as suggestive significant pleiotropic SNPs. The independent SNPs were defined using LD clumping with 250 kb and an  $r^2$  threshold of 0.1, utilizing the 1000 Genomes European ancestry data as the reference panel (EUR-LD reference).

*Pleiotropic SNPs associated with SCZ and CMR phenotypes.* We found a total of 437 unique significant independent pleiotropic SNPs between SCZ and 28 CMR phenotypes (Fig. 3a and Supplementary Table 8). Specifically, there were 170 pleiotropic SNPs for the left ventricle (LV), 71 SNPs for the right ventricle (RV), 48 SNPs left atrium (LA), 70 SNPs for the right atrium (RA), 76 SNPs for the ascending aorta (AAo), and 53 SNPs for the descending aorta (DAo). For example, rs71395455 exhibited a pleiotropic effect between SCZ and global myocardial-wall thickness at end-diastole ( $P_{PLACO} = 1.57 \times 10^{-20}$ ); rs2224770 displayed a significant pleiotropic effect between SCZ and the minimum area of the ascending aorta ( $P_{PLACO} = 8.80 \times 10^{-16}$ ). Among all the 28 CMR phenotypes analyzed, the ascending aorta maximum area and minimum area revealed the highest number of pleiotropic SNPs, with 46 and 48 pleiotropic SNPs, respectively. Additionally, among the 437 significant SNPs identified by PLACO, 144 (33.0%) were novel findings compared with the original GWAS for each phenotype ( $P < 5 \times 10^{-8}$ ).

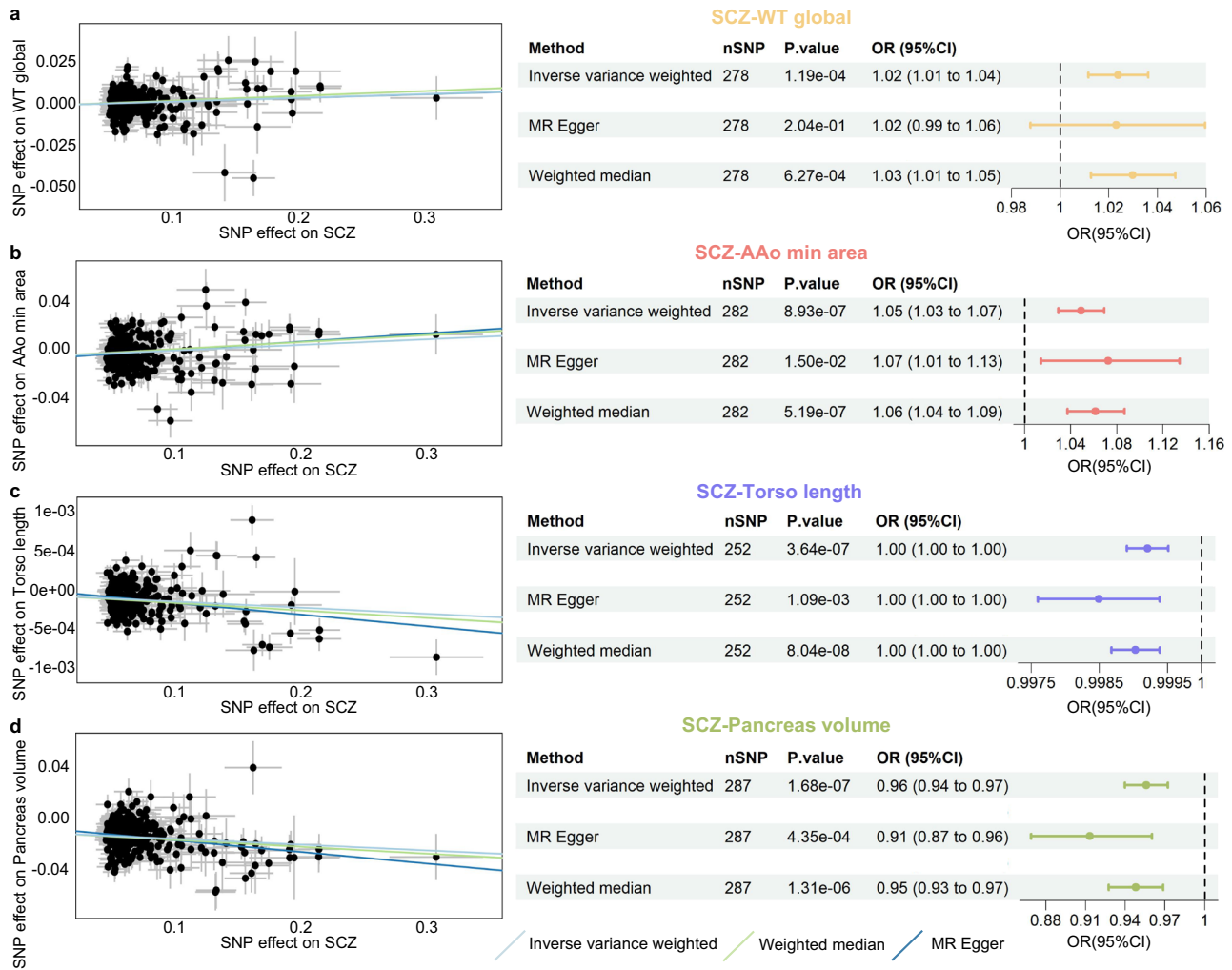


**Fig. 2 Causal associations between SCZ and peripheral organ imaging phenotypes.** The detailed results for MR analyses between SCZ and WT global (a) AAO min area (b) torso length (c) and pancreas volume (d) are shown for each MR method. Each point on the left panel represents an individual SNP with its effect size on SCZ (x-axis) and imaging phenotype (y-axis), and each line demonstrates one MR method. AAO min area ascending aorta minimum area, OR odds ratio, SCZ schizophrenia, SNP single nucleotide polymorphism, WT global global myocardial-wall thickness at end-diastole, 95% CI 95% confidence interval.

**Pleiotropic SNPs associated with SCZ and skeletal DXA phenotypes.** We found a total of 257 unique significant independent pleiotropic SNPs between SCZ and skeletal DXA phenotypes (Fig. 3b and Supplementary Table 9). Specifically, we identified 42 pleiotropic SNPs for femur length, 51 SNPs for forearm length, 29 SNPs for humerus length, 54 SNPs for tibia length, 16 SNPs for tibiofemoral angle, 32 SNPs for hip width, 25 SNPs for shoulder width, and 43 SNPs for torso length. Besides, of the 257 pleiotropic SNPs, 85 (33.1%) were novel findings compared with the original GWAS for each phenotype ( $P < 5 \times 10^{-8}$ ). The most significant finding was the pleiotropic effect of rs13107511 for femur length with a  $P_{PLACO}$  of  $9.03 \times 10^{-18}$ . Additionally, rs10950415 showed a significant pleiotropic effect with forearm length ( $P_{PLACO} = 1.03 \times 10^{-15}$ ), while rs13135092 displayed significant pleiotropic effects with both humerus length ( $P_{PLACO} = 1.50 \times 10^{-15}$ ) and torso length ( $P_{PLACO} = 2.45 \times 10^{-14}$ ).

**Pleiotropic SNPs associated with SCZ and abdominal MRI phenotypes.** A total of 230 significant independent pleiotropic SNPs were identified between SCZ and abdominal MRI phenotypes (Fig. 3c and Supplementary Table 10). Specifically, there were 33 SNPs for visceral adipose tissue, 32 SNPs for spleen volume, 27 SNPs for pancreas volume, 26 SNPs for liver fat content and liver volume, 24

SNPs for kidney volume, 23 SNPs for liver iron content, 20 SNPs for lung volume, 20 SNPs for abdominal subcutaneous adipose tissue, 16 SNPs for pancreas fat content, and 9 SNPs for pancreas iron content. For example, rs3934667 showed a significant pleiotropic effect with liver fat ( $P_{PLACO} = 2.89 \times 10^{-21}$ ). Similarly, among the 230 significant SNPs detected by PLACO, 67 (29.1%) were not deemed significant in the individual original GWAS for either phenotype ( $P < 5 \times 10^{-8}$ ).

#### Functional annotations for pleiotropic SNPs and genes

FUMA (<https://fuma.ctglab.nl>)<sup>32</sup> was used to perform the SNP-level annotations for these pleiotropic SNPs, using Combined Annotation Dependent Depletion (CADD) scores, regulomeDB (RDB) scores, and minChrState values. CADD scores assess the disease potential of SNPs<sup>33</sup>, RDB scores evaluate their possible regulatory functions<sup>34</sup>, and minChrState indicates whether the SNPs are located within open and transcriptionally active chromatin regions<sup>35</sup>. For unique SNPs shared by SCZ and CMR phenotypes, the majority of SNPs (60.9%) were located within intronic regions, while 16 SNPs were located within exonic regions, and the rest were distributed across other regions. Furthermore, 25 SNPs had CADD scores above 12.37, with rs11692435 having the highest score at 28.3. Additionally, 26 SNPs with RDB scores of 1b to 1f,

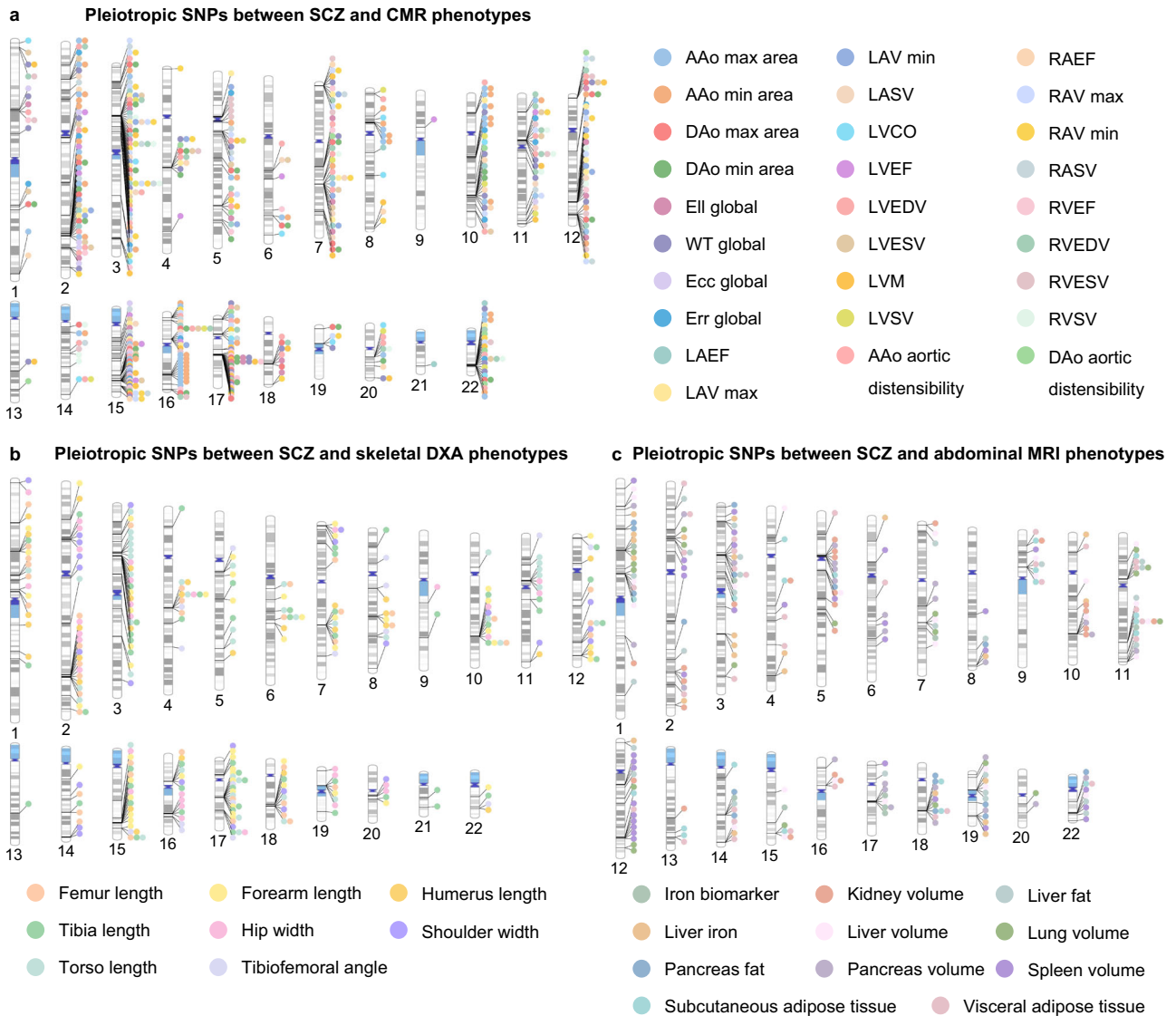


**Fig. 3 The genomic location of pleiotropic SNPs between SCZ and peripheral organ imaging phenotypes identified by PLACO.** The genomic locations of pleiotropic SNPs are shown, including 437 pleiotropic SNPs between SCZ and 28 CMR phenotypes (a) 257 pleiotropic SNPs between SCZ and eight skeletal DXA phenotypes (b) and 230 pleiotropic SNPs between SCZ and 11 abdominal MRI phenotypes c. AAo aortic distensibility ascending aorta distensibility, AAo max area ascending aorta maximum area, AAo min area ascending aorta minimum area, CMR cardiac magnetic resonance, DAo aortic distensibility descending aorta distensibility, DAo max area descending aorta maximum area, DAo min area descending aorta minimum area, DXA dual-energy X-ray absorptiometry, Ecc global global peak circumferential strain, Ell global global longitudinal strain, Err global global radial strain, LAEF left atrium ejection fraction, LASV left atrium stroke volume, LAV max left atrium maximum volume, LAV min left atrium minimum volume, LVCO left ventricular cardiac output, LVEDV left ventricular end-diastolic volume, LVEF left ventricular ejection fraction, LVESV left ventricular end-systolic volume, LVM left ventricular myocardial mass, LVSV left ventricular stroke volume, MRI magnetic resonance imaging, PLACO pleiotropic analysis under composite null hypothesis, RAEF right atrium ejection fraction, RASV right atrium stroke volume, RAV max right atrium maximum volume, RAV min right atrium minimum volume, RVEDV right ventricular end-diastolic volume, RVEF right ventricular ejection fraction, RVESV right ventricular end-systolic volume, RVSV right ventricular stroke volume, SCZ schizophrenia, SNP single nucleotide polymorphism, WT global global myocardial-wall thickness at end-diastole.

and 412 SNPs showing a minChrState value < 8 (Supplementary Table 11). For unique SNPs shared by SCZ and skeletal DXA phenotypes, the primary location was also within intronic regions (55.3%), and notably eight SNPs were located within exonic regions. Furthermore, 28 SNPs had CADD scores above 12.37, with rs3764002 having the highest score at 28.1. Besides, 14 SNPs with RDB scores of 1b to 1f, and 236 SNPs showing a minChrState value < 8 (Supplementary Table 12). Regarding unique SNPs shared by SCZ and abdominal MRI phenotypes, the primary location of the candidate SNPs was within intronic regions (46.5%), with seven SNPs located within exonic regions. Furthermore, 11

SNPs had CADD scores above 12.37, among which rs114165349 recorded the highest score of 22.1. Additionally, six SNPs with RDB scores of 1b to 1f, and 200 SNPs showing a minChrState value < 8 (Supplementary Table 13). The distributions of the CADD scores for these pleiotropic SNPs are shown in Supplementary Fig. 3, and functional consequence, RDB scores, and minChrState values for these pleiotropic SNPs are displayed in Fig. 4a–c.

Furthermore, we utilized the ToppGene (<http://toppgene.cchmc.org>)<sup>36</sup> to delve into the critical biological processes based on the nearest genes of identified pleiotropic SNPs between SCZ and peripheral organ imaging phenotypes,

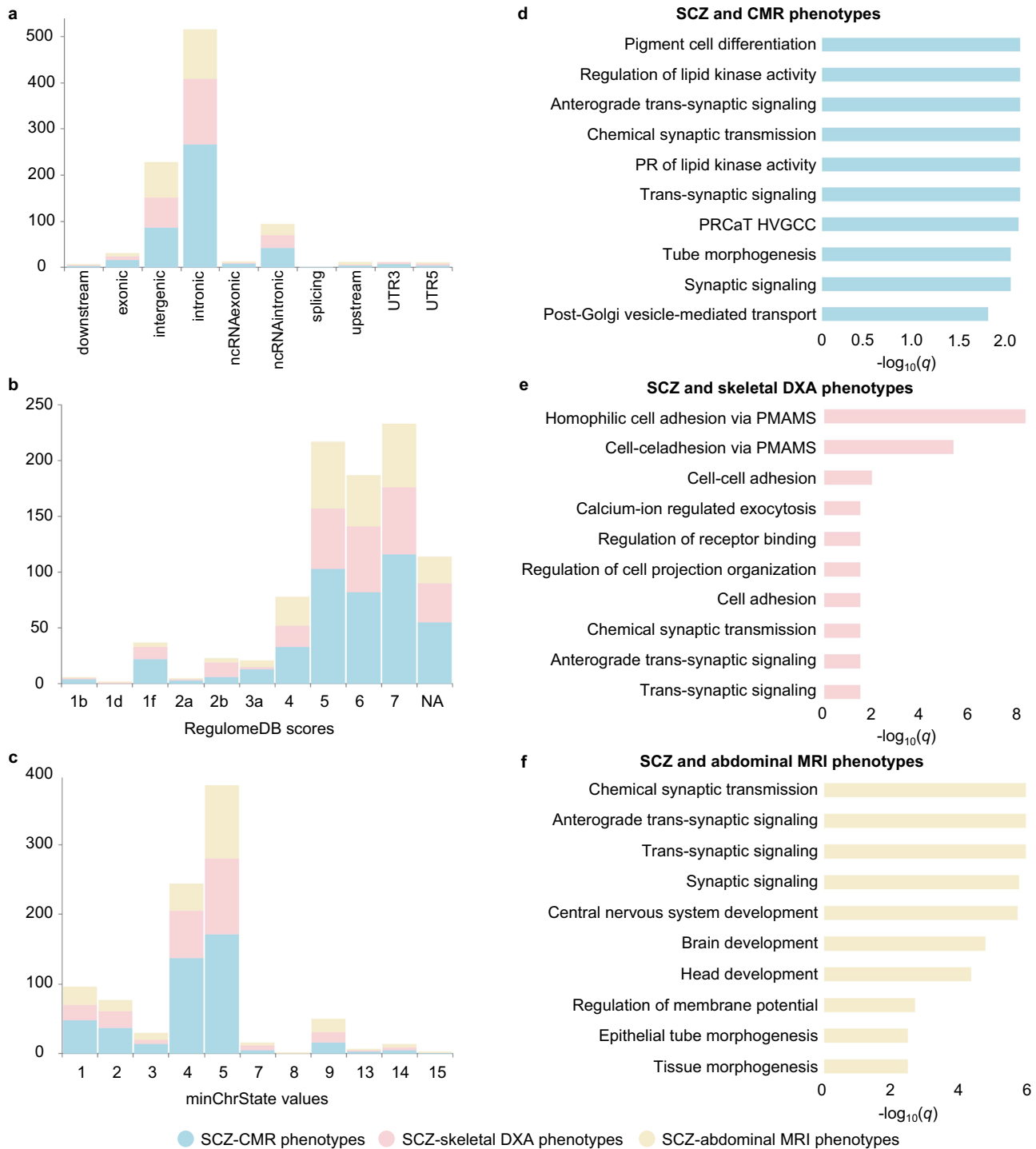


**Fig. 4 Functional annotations for pleiotropic SNPs and genes between SCZ and peripheral organ imaging phenotypes.** **a–c** The SNP annotations for the derived pleiotropic SNPs. Different color represents different organ group (CMR phenotypes, skeletal DXA phenotypes, and abdominal MRI phenotypes). **d–f** The top 10 significantly enriched biological processes are shown based on shared genes between SCZ and CMR phenotypes, skeletal DXA phenotypes, and abdominal MRI phenotypes. The x-axis shows the  $-\log_{10}(q)$  for each biological process. CMR cardiac magnetic resonance, DXA dual-energy X-ray absorptiometry, MRI magnetic resonance imaging, PMAMS plasma membrane adhesion molecules, PR positive regulation, PRCaT HVGCC positive regulation of calcium ion transmembrane transport via high voltage-gated calcium channel, SCZ schizophrenia.

with significance determined by FDR-BH correction ( $q < 0.05$ ). For the pleiotropic genes shared by SCZ and CMR phenotypes, 44 significant biological processes were identified ( $q < 0.05$ , Supplementary Table 14 and Fig. 4d), such as the regulation of lipid kinase activity (GO:0043550,  $q = 6.69 \times 10^{-3}$ ). Additionally,

18 significant biological processes were identified based on pleiotropic genes shared by SCZ and skeletal DXA phenotypes, and 99 significant biological processes for abdominal MRI phenotypes (Supplementary Table 14 and Fig. 4e, f). For example, the negative regulation of the hydrogen peroxide catabolic

process (GO:2000296,  $q = 3.41 \times 10^{-2}$ ) was one of the key biological processes for genes shared by SCZ and skeletal DXA phenotypes, which plays an important role in both bone health and SCZ<sup>45,46</sup>. Specially, synapse-related biological processes were significantly enriched across all three groups of organ imaging phenotypes ( $q < 0.05$ ), such as anterograde trans-synaptic signaling, chemical synaptic transmission, trans-synaptic signaling, and synaptic signaling, which suggested the importance of synapse in the etiology and pathology of SCZ and the comorbidity with peripheral organ dysfunctions.

### Cognitive associations

We performed phenotype-wide association analyses with eight cognitive phenotypes consistent with a previous study based on the pleiotropic SNPs shared between SCZ and CMR phenotypes, skeletal DXA phenotypes, and abdominal MRI phenotypes, respectively (Supplementary Table 2). We defined a SNP as phenotype-wide significant if it reached genome-wide significance ( $P < 5 \times 10^{-8}$ ) in the GWAS of any of the eight cognitive phenotypes. The results showed that a subset of the pleiotropic SNPs shared between SCZ and CMR, skeletal DXA, or abdominal MRI phenotypes showed significant associations with cognitive abilities, with 18, 11, and 8 SNPs meeting this criterion, respectively (Supplementary Fig. 4 and Supplementary Table 15).

### Cell-type enrichment analysis

We have performed the cell-type enrichment analysis using the bioinformatics tool WebCSEA (<https://bioinfo.uth.edu/webcsea/submit.php>)<sup>38</sup>. For the pleiotropic SNPs between SCZ and CMR phenotypes, cell-type enrichment analysis revealed excitatory neurons as the most significantly enriched ( $P = 3.03 \times 10^{-4}$ ), followed by inhibitory neurons ( $P = 4.83 \times 10^{-4}$ ) and Purkinje cells ( $P = 4.86 \times 10^{-4}$ ) (Supplementary Fig. 5a). For those between SCZ and skeletal DXA phenotypes, the club cell showed the highest enrichment ( $P = 1.17 \times 10^{-3}$ ), followed by excitatory neurons ( $P = 1.21 \times 10^{-3}$ ) and neurons ( $P = 2.14 \times 10^{-3}$ ) (Supplementary Fig. 5b). For the pleiotropic SNPs between SCZ and abdominal MRI phenotypes, excitatory neurons were the most enriched cell type ( $P = 1.06 \times 10^{-4}$ ) (Supplementary Fig. 5c).

### Spatio-temporal gene expression trajectory analysis

Understanding when and where this shared genetic architecture is expressed during critical developmental windows or in adulthood can provide valuable insights into the molecular mechanisms driving both SCZ and peripheral organ dysfunctions. The spatio-temporal patterns of brain gene expression for genes shared between SCZ and each group of peripheral organ imaging phenotypes were identified using mRNA-seq data from PsychENCODE<sup>39,40</sup>. The averaged expression of shared genes associated with CMR phenotypes and SCZ in the whole brain showed a higher level of expression compared to those linked to the other two organ groups of imaging phenotypes throughout the lifespan (Fig. 5a). Furthermore, for the shared genes associated with CMR phenotypes and skeletal DXA phenotypes, the averaged expression in the whole brain exhibited an initial increase followed by a decrease, with peak expression occurring during the 16–22 post-conception weeks (PCW) stage. This may suggest that this developmental window is critical for both SCZ and the dysfunctions observed in the heart and skeleton. In contrast, the shared genes linked to abdominal MRI phenotypes demonstrated a continuous increase in expression over time (Fig. 5b–d).

### Drugs targeting the identified pleiotropic genes

Drug enrichment analyses and drug-gene interaction studies offer promising avenues for therapeutic development. By identifying drugs that target these shared genetic pathways, it is possible to

repurpose existing treatments or develop new interventions that address both the psychiatric and systemic aspects of SCZ. The Genome for REPositioning drugs (GREP, <https://github.com/saorisakaue/GREP>)<sup>41</sup> methodology was used to identify the drugs targeting the identified pleiotropic genes between SCZ and peripheral organ imaging phenotypes (Fig. 6a and Supplementary Table 16). Two significant enrichment groups of drugs were identified for genes shared by SCZ and CMR phenotypes, such as the marked enrichment of calcium channel blockers (C08; odds ratio = 16.032, Fisher's Exact Test  $P = 2.83 \times 10^{-4}$ ). Besides, three significant enrichment groups of drugs were identified for skeletal DXA phenotypes; the most significant one was the enrichment of calcium channel blockers (C08; odds ratio = 17.55, Fisher's Exact Test  $P = 0.001$ ). For genes shared by SCZ and abdominal MRI phenotypes, five significant enrichment groups of drugs were identified. The most significant one was drugs for functional gastrointestinal disorders (A03; odds ratio = 15.445, Fisher's Exact Test  $P = 3.31 \times 10^{-4}$ ).

We analyzed the drug-gene interactions (DGIs) of the identified pleiotropic genes using the drug-gene interaction database (DGIdb, <https://www.dgiddb.org>)<sup>44</sup>, and interactions were defined as the interaction score larger than zero. We only retained the drugs involved in the library of GREP. For genes shared by SCZ and CMR phenotypes, we found 36 unique genes that interacted with 142 drugs (Supplementary Table 17). Notably, *MAPT* showed the most number of unique drugs ( $n = 30$ ), followed by *CACNA1C* ( $n = 20$ ), *THRB* ( $n = 15$ ), *CACNA1D* ( $n = 12$ ), and *CACNA1I* ( $n = 12$ ). These drugs encompassed various classes, including inhibitors, agonists, blockers, and modulators. For genes shared by SCZ and skeletal DXA phenotypes, we found 21 unique genes that interacted with 131 drugs (Supplementary Table 18). For genes shared by SCZ and abdominal MRI phenotypes, 25 unique genes interacted with 321 drugs (Supplementary Table 19), with *ABCB1* topping the list, interacting with 178 drugs. The top ten interactions with the highest interaction group scores are shown in Fig. 6b–d.

## DISCUSSION

In this study, we explored the shared genetic architecture between SCZ and multiple peripheral organ systems using imaging phenotypes derived from CMR, skeletal DXA, and abdominal MRI. We identified the causal associations between SCZ and each of the common peripheral imaging phenotypes and revealed pleiotropic SNPs between SCZ and various peripheral organ systems, which shed light on the broader physiological manifestations often observed in SCZ patients. Critical biological processes were uncovered, especially for synapse-related functions. In addition, distinct spatio-temporal expression patterns in the brain were characterized based on genes shared between SCZ and organ group-specific imaging phenotypes. Furthermore, we investigated enrichments and interactions between shared genes and drugs. Collectively, these findings contribute to a deeper understanding of the intricate relationship between SCZ and multi-systemic health in various organ domains, offering valuable insights into the biology of SCZ and potential new treatment approaches.

By using the MR approach, our findings revealed significant positive causal relationships between SCZ and WT global, AAO min area, AAO max area, and LVM. These results are consistent with previous studies that have indicated an increased risk of cardiovascular abnormalities in SCZ patients<sup>2,3</sup>. A large-scale meta-analysis revealed that for people with severe mental illness (including SCZ), there was a statistically significant increase in the incidence of various cardiovascular conditions. Specifically, the incidence of coronary artery disease rose by 54%, cerebrovascular disease by 64%, congestive heart failure by 110%, and the risk of cardiovascular-related death increased by 85%<sup>47</sup>. These findings

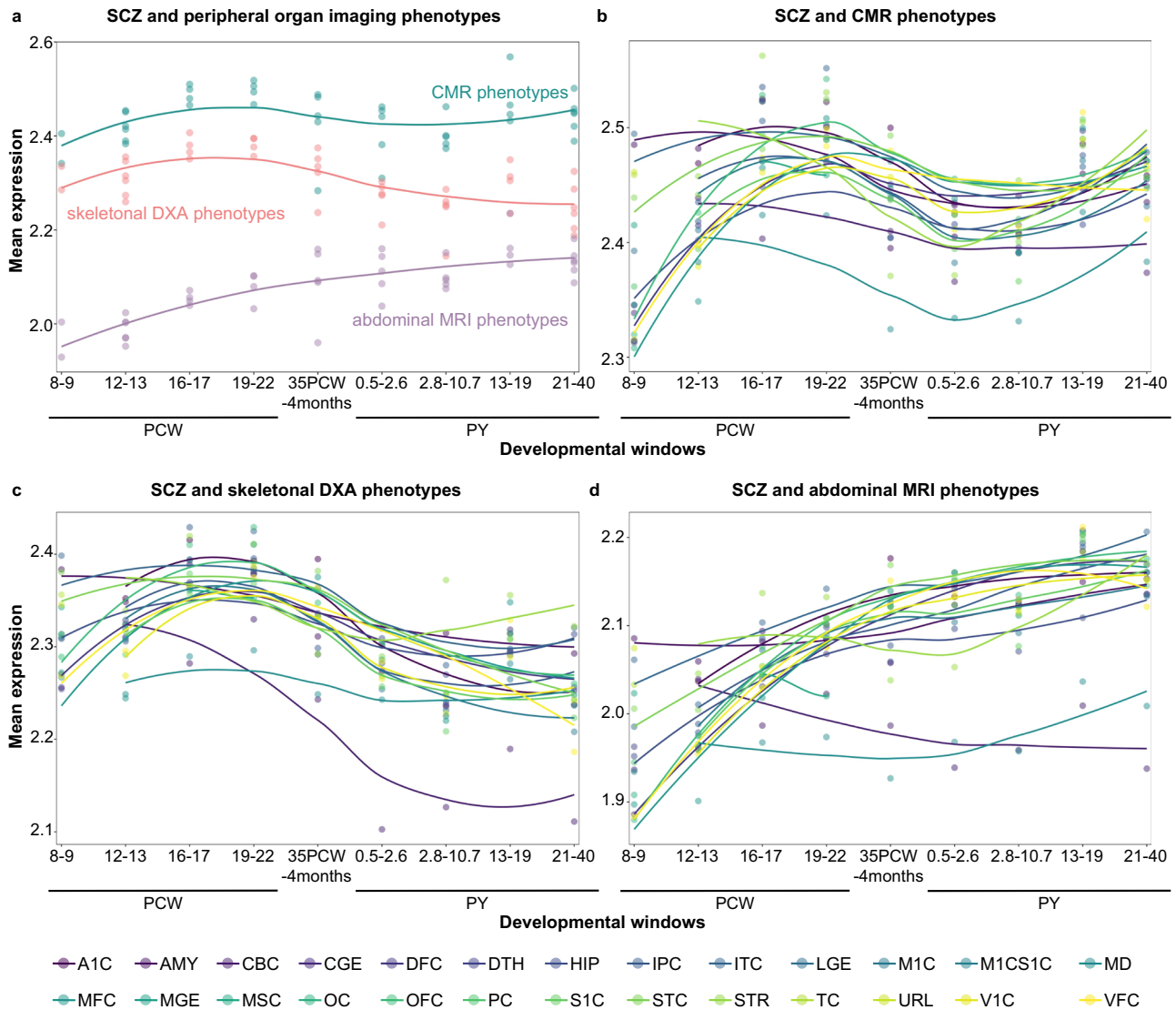


**Fig. 5 Spatio-temporal gene expression analysis for genes shared between SCZ and peripheral organ imaging phenotypes.** **a** The spatio-temporal patterns of average gene expression in the whole brain for genes shared between SCZ and peripheral organ imaging phenotypes. The color of the bubbles and lines denotes different organ imaging phenotypes. **b-d** The spatio-temporal patterns of gene expression in the whole brain for genes shared between SCZ and each group of peripheral organ imaging phenotypes. The x-axis represents the nine developmental windows, and the y-axis represents the log<sub>2</sub>-transformed and normalized mean expression value. The color of the bubbles and lines denotes different brain regions and neocortical areas. A1C primary auditory cortex, AMY amygdala, CBC cerebellar cortex, CGE caudal ganglionic eminence, CMR cardiac magnetic resonance, DFC dorsolateral prefrontal cortex, DTH dorsal part of the thalamic anlage, DXA dual-energy X-ray absorptiometry, HIP hippocampus, IPC posterior inferior parietal cortex, ITC inferior temporal cortex, LGE lateral ganglionic eminence, M1C primary motor cortex, M1CS1C motor-somatosensory cortex, MD thalamus, MFC medial prefrontal cortex, MGE medial ganglionic eminence, MRI magnetic resonance imaging, MSC motor and somatosensory cortex, OC occipital cortex, OFC orbital prefrontal cortex, PC parietal cortex, PCW post-conception week, PY postnatal year, S1C primary somatosensory cortex, SCZ schizophrenia, STC posterior superior temporal cortex, STR striatum, TC temporal cortex, URL upper (rostral) rhombic lip, V1C primary visual cortex, VFC ventrolateral prefrontal cortex.

collectively suggest that SCZ may profoundly impact the cardiovascular system through alterations in cardiac structure and function<sup>2,3</sup>. Additionally, we observed negative causal effects for SCZ on the measurements of torso length, pancreas volume, and subcutaneous adipose tissue. These changes in body morphology and composition likely reflect broader alterations in metabolism and nutritional status among individuals with SCZ, providing new insights into the link between SCZ and systemic metabolic dysfunction. Furthermore, our analysis identified several genomic regions (LD blocks) with significant genetic correlations between SCZ and imaging phenotypes, further elucidating the

complex interplay between genetic factors and peripheral organ health. For example, LD block 101 (chr1: 114,664,388–116,207,297) demonstrated a significant correlation with descending aorta distensibility and SCZ. The *NGF* is located in the region, which is a crucial regulator in the development and maintenance of the nervous system, playing a pivotal role in neuronal survival and synaptic plasticity<sup>48</sup>. Additionally, LD block 2,084 (chr15: 84,209,761–85,494,083) was linked to the global myocardial-wall thickness at end-diastole and SCZ. The *ALPK3* is located in the region, with multiple studies emphasizing the close association between the *ALPK3* locus and the occurrence of hypertrophic

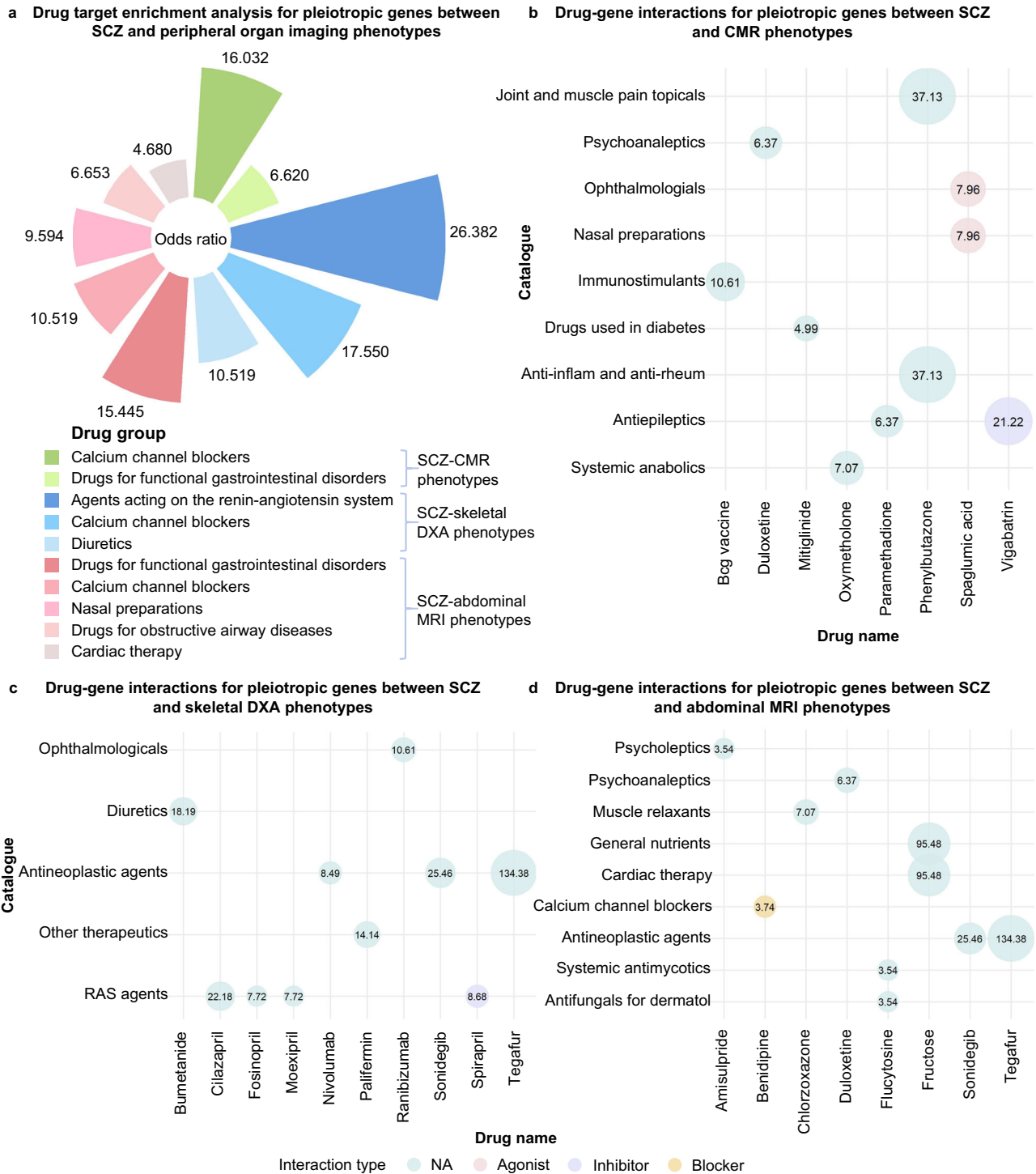


**Fig. 6 Drug-target enrichment analysis and gene-drug interactions.** **a** The significant results (Fisher's Exact Test  $P < 0.05$ ) of drug-target enrichment analyses based on shared genes between SCZ and peripheral organ imaging phenotypes using GREP. The bar chart depicts the odds ratios (ORs) of various drug groups across three organ groups of imaging phenotypes (CMR phenotypes, skeletal DXA phenotypes, and abdominal MRI phenotypes). Each drug group is distinguished by a unique color. **b-d** The bubble plots illustrated the drug-gene interactions for genes shared between SCZ and three organ groups of imaging phenotypes (CMR phenotypes, skeletal DXA phenotypes, and abdominal MRI phenotypes) using the DGldb. The x-axis represents drug names, the y-axis indicates drug categories, and the size of the bubbles reflects the drug-gene interaction group score, a quantitative measure of the strength or significance of the interactions. The color of the bubbles denotes different drug-gene interaction types. CMR cardiac magnetic resonance, DGldb the Drug Gene Interaction Database, DXA dual-energy X-ray absorptiometry, GREP the Genome for REPositioning Drugs, MRI magnetic resonance imaging, RAS renin-angiotensin system, SCZ schizophrenia.

cardiomyopathy (HCM)<sup>49,50</sup>. In summary, these findings underscore the intricate genetic and causal relationships between SCZ and peripheral organ imaging phenotypes, providing novel insights into the complex pathological mechanisms underlying SCZ and its systemic manifestations.

On the other hand, we uncovered pleiotropic SNPs shared between SCZ and each of the peripheral organ imaging phenotypes. Notably, the maximum and minimum areas of the AAo show the highest number of pleiotropic SNPs. For example, rs13135092 was shared between SCZ and both humerus length and torso length; the nearest gene was *SLC39A8*. Some missense variants in *SLC39A8* were convincingly associated with SCZ<sup>51,52</sup>. Furthermore, we have identified two SNPs, rs77882218 and rs79780963, that are shared across SCZ and three groups of organ imaging phenotypes. The nearest genes were *RP11-397A16.1* and *NT5C2*, respectively. The *NT5C2* (5'-nucleotidase cytosolic II) gene has been identified as a robust susceptibility gene for SCZ through large-scale GWAS<sup>53</sup>. Moreover, synapse-related biological processes show significant associations with genes shared between SCZ and all three organ group-specific phenotypes, which have been demonstrated to be closely related to the risk of developing SCZ<sup>14,54</sup>. In addition, rs3764002 was shared by SCZ and torso length, which is a new finding compared with the original GWAS, with a CADD score of 28.1. It indicated that PLACO may enhance the power to detect shared genetic signals by aggregating evidence across related phenotypes. Furthermore, some of the pleiotropic SNPs were associated with cognitive abilities, which indicates genetic variants that not only shared between SCZ and peripheral organ phenotypes, but also likely linked to cognitive changes in SCZ patients. For biological pathways, previous studies have shown that the expression of synaptic function-related genes like *RIMS1* and *SLC18A2* in adipose tissue correlates with cognitive function<sup>55</sup>. Furthermore, preganglionic sympathetic neurons release acetylcholine at synaptic junctions in peripheral ganglia, mirroring classical neurotransmission in the brain<sup>56</sup>. Similarly, studies indicated that sympathetic neurons communicate with cardiomyocytes via structured intercellular interactions called neuro-cardiac junctions, which are functionally analogous to the neuromuscular junction in skeletal muscle<sup>57,58</sup>. These processes are coordinated by central nuclei such as the hypothalamus and brainstem, which project to preganglionic neurons, illustrating a direct synaptic continuum between central nervous system (CNS) command centers and peripheral effector organs<sup>59</sup>. Thus, synaptic dysfunction in neuropsychiatric disorders may disrupt autonomic nervous system (ANS)-mediated peripheral homeostasis, acting as a critical mechanistic bridge between central pathology and systemic phenotypes. Furthermore, the enteric nervous system (ENS) in the autonomic nervous system achieves autonomous regulation of intestinal functions, and at the same time interacts with the CNS via a neuro-humoral combined mechanism<sup>60</sup>.

Distinct spatio-temporal expression patterns in the brain were clarified based on shared genes between SCZ and imaging phenotypes from CMR, skeletal DXA, and abdominal MRI. For CMR and skeletal DXA imaging phenotypes, shared genes exhibited peak expression during the 16–22 PCW time window, suggesting a critical period of heightened gene activity that may be pivotal for SCZ, cardiovascular, and skeletal development. In contrast, shared genes derived from abdominal MRI phenotypes showed an increasing expression trend throughout the lifespan, indicating ongoing relevance and potential changes in gene function associated with metabolic and organ group-specific processes over time. These findings underscore the dynamic and developmental aspects of gene expression related to SCZ, offering valuable insights into the temporal and spatial dimensions of the disorder's impact on peripheral organ systems.

The significance of drug-gene enrichment analysis lies in its ability to reveal actionable insights into the systemic impact of

SCZ on peripheral organ health, which can inform therapeutic strategies. For instance, the identification of calcium channel blockers (C08) in the enrichment analysis highlights a crucial link between SCZ and an increased risk of cardiovascular complications. This finding suggested that integrating treatments such as calcium channel blockers could help manage and mitigate cardiovascular risks associated with SCZ<sup>61</sup>. Moreover, DGIs revealed intricate connections between a series of key genes and medications. For instance, the *CACNA1C* plays a pivotal role in the pathology of psychiatric disorders<sup>62,63</sup>. Together, these findings not only enhance our understanding of SCZ's peripheral organ effects but also offer practical implications for optimizing patient care and treatment strategies.

There are several limitations that need to be considered. Firstly, our study included only three major categories of peripheral organs due to the available large-scale GWAS summary data, and a wider range of peripheral organs could help to better capture the comprehensive systemic dysfunction of SCZ. Secondly, some of the MR analyses revealed significant heterogeneity, although high heterogeneity does not necessarily indicate bias or unreliable results<sup>64</sup>. Thirdly, our analyses were based on data from individuals of EUR ancestry, and the applicability of these findings to other ethnic groups requires further validation. Fourthly, while gene expression trends are generally consistent across most brain regions, region-specific heterogeneity exists—and unequal sampling density in reference transcriptomic datasets may bias curve fitting and data interpretability. Finally, although our drug enrichment analysis highlighted potential candidates of therapeutic interest, these findings are preliminary and based solely on in silico predictions derived from pleiotropic genetic signals. The clinical relevance and therapeutic efficacy of these agents in the context of SCZ and its related peripheral phenotypes remain to be validated. Therefore, further experimental studies, advanced molecular techniques in psychiatric disorders<sup>65</sup>, and prospective clinical investigations are essential to confirm their biological impact and translational potential.

Overall, our study provides significant insights into the intricate genetic relationship between SCZ and peripheral organ dysfunctions, elucidating how genetic factors contribute to the disorder's extensive physiological impact. By integrating genetic data with disorder and imaging phenotypes, we have uncovered critical associations that pave the way for more targeted and effective therapeutic strategies. This comprehensive approach not only enhances our understanding of the multifaceted nature of SCZ but also underscores the necessity for holistic management strategies. Such strategies should encompass both psychiatric and systemic health aspects, addressing the broad spectrum of challenges faced by SCZ patients and ultimately improving their overall well-being and treatment outcomes.

Received: 18 May 2025; Accepted: 18 August 2025;

Published online: 29 September 2025

## REFERENCES

1. Global Burden of Disease Study 2013 Collaborators Global, regional, and national incidence, prevalence, and years lived with disability for 301 acute and chronic diseases and injuries in 188 countries, 1990–2013: a systematic analysis for the Global Burden of Disease Study 2013. *Lancet* **386**, 743–800 (2015).
2. Osimo, E. F. et al. Cardiac structure and function in schizophrenia: cardiac magnetic resonance imaging study. *Br. J. Psychiatry* **217**, 450–457 (2020).
3. Pillinger, T. et al. Effect of polygenic risk for schizophrenia on cardiac structure and function: a UK Biobank observational study. *Lancet Psychiatry* **10**, 98–107 (2023).
4. Gomez, L. et al. Lower Bone Mineral Density At The Hip And Lumbar Spine In People With Psychosis Versus Controls: A Comprehensive Review And Skeletal Site-specific Meta-analysis. *Curr. Osteoporos. Rep.* **14**, 249–259 (2016).

5. Partti, K. et al. Skeletal status in psychotic disorders: a population-based study. *Psychosom. Med.* **72**, 933–940 (2010).
6. Galiano Rus, S. et al. Elevated risk of liver steatosis in first-episode psychosis patients: Results from a 3-year prospective study. *Schizophr. Res.* **246**, 30–38 (2022).
7. Owiredu, W. et al. Evaluation of serum iron overload, AST:ALT ratio and log(10) ferritin:AST ratio among schizophrenia patients in the Kumasi Metropolis, Ghana: a case-control study. *BMC Res. notes* **12**, 802 (2019).
8. Konarzewska, B. et al. Visceral obesity in normal-weight patients suffering from chronic schizophrenia. *BMC Psychiatry* **14**, 35 (2014).
9. DE Hert, M. et al. Physical illness in patients with severe mental disorders. I. Prevalence, impact of medications and disparities in health care. *World Psychiatry* **10**, 52–77 (2011).
10. Sullivan, P. F., Kendler, K. S. & Neale, M. C. Schizophrenia as a complex trait: evidence from a meta-analysis of twin studies. *Arch. Gen. Psychiatry* **60**, 1187–1192 (2003).
11. Sullivan, P. F. et al. Psychiatric genomics: an update and an agenda. *Am. J. Psychiatry* **175**, 15–27 (2018).
12. Kun, E. et al. The genetic architecture and evolution of the human skeletal form. *Science* **381**, eadf8009 (2023).
13. Liu, Y. et al. Genetic architecture of 11 organ traits derived from abdominal MRI using deep learning. *eLife* <https://doi.org/10.7554/eLife.65554> (2021).
14. Trubetskoy, V. et al. Mapping genomic loci implicates genes and synaptic biology in schizophrenia. *Nature* **604**, 502–508 (2022).
15. Zhao, B. et al. Heart-brain connections: Phenotypic and genetic insights from magnetic resonance images. *Science* **380**, abn6598 (2023).
16. Xie, Y. et al. Genetic and neural mechanisms shared by schizophrenia and depression. *Mol. Psychiatry* <https://doi.org/10.1038/s41380-025-02975-5> (2025).
17. Xie, Y. et al. Shared genetic architecture among gastrointestinal diseases, schizophrenia, and brain subcortical volumes. *Schizophr. Bull.* **50**, 1243–1254 (2024).
18. Zhao, Q. et al. Genome-wide pleiotropy analysis reveals shared genetic associations between type 2 diabetes mellitus and subcortical brain volumes. *Research* **8**, 0688 (2025).
19. Konzok, J. et al. Child maltreatment as a transdiagnostic risk factor for the externalizing dimension: a Mendelian randomization study. *Mol. Psychiatry* <https://doi.org/10.1038/s41380-024-02700-8> (2024).
20. Li, R. et al. An observational and genetic investigation into the association between psoriasis and risk of malignancy. *Nat. Commun.* **15**, 7952 (2024).
21. Rasheed, H. et al. The causal effects of serum lipids and apolipoproteins on kidney function: multivariable and bidirectional Mendelian-randomization analyses. *Int. J. Epidemiol.* **50**, 1569–1579 (2021).
22. Wang, W. et al. Unraveling the causal relationships between depression and brain structural imaging phenotypes: a bidirectional Mendelian Randomization study. *Brain Res.* **1840**, 149049 (2024).
23. Werme, J., van der Sluis, S., Posthuma, D. & de Leeuw, C. A. An integrated framework for local genetic correlation analysis. *Nat. Genet.* **54**, 274–282 (2022).
24. Ray, D. & Chatterjee, N. A. powerful method for pleiotropic analysis under composite null hypothesis identifies novel shared loci between type 2 diabetes and prostate cancer. *PLoS Genet.* **16**, e1009218 (2020).
25. Hemani, G. et al. The MR-Base platform supports systematic causal inference across the human phenome. *eLife* <https://doi.org/10.7554/eLife.34408> (2018).
26. Hemani, G., Tilling, K. & Davey Smith, G. Orienting the causal relationship between imprecisely measured traits using GWAS summary data. *PLoS Genet.* **13**, e1007081 (2017).
27. Bowden, J. et al. Improving the accuracy of two-sample summary-data Mendelian randomization: moving beyond the NOME assumption. *Int. J. Epidemiol.* **48**, 728–742 (2019).
28. Greco, M. F., Minelli, C., Sheehan, N. A. & Thompson, J. R. Detecting pleiotropy in Mendelian randomisation studies with summary data and a continuous outcome. *Stat. Med.* **34**, 2926–2940 (2015).
29. Burgess, S., Butterworth, A. & Thompson, S. G. Mendelian randomization analysis with multiple genetic variants using summarized data. *Genet. Epidemiol.* **37**, 658–665 (2013).
30. Bowden, J., Davey Smith, G., Haycock, P. C. & Burgess, S. Consistent estimation in Mendelian randomization with some invalid instruments using a weighted median estimator. *Genet. Epidemiol.* **40**, 304–314 (2016).
31. Ray, D. et al. Pleiotropy method reveals genetic overlap between orofacial clefts at multiple novel loci from GWAS of multi-ethnic trios. *PLoS Genet.* **17**, e1009584 (2021).
32. Watanabe, K., Taskesen, E., van Bochoven, A. & Posthuma, D. Functional mapping and annotation of genetic associations with FUMA. *Nat. Commun.* **8**, 1826 (2017).
33. Rentzsch, P., Witten, D., Cooper, G. M., Shendure, J. & Kircher, M. CADD: predicting the deleteriousness of variants throughout the human genome. *Nucleic Acids Res.* **47**, D886–d894 (2019).
34. Boyle, A. P. et al. Annotation of functional variation in personal genomes using RegulomeDB. *Genome Res.* **22**, 1790–1797 (2012).
35. Ernst, J. & Kellis, M. ChromHMM: automating chromatin-state discovery and characterization. *Nat. Methods* **9**, 215–216 (2012).
36. Chen, J., Bardes, E. E., Aronow, B. J. & Jegga, A. G. ToppGene Suite for gene list enrichment analysis and candidate gene prioritization. *Nucleic Acids Res.* **37**, W305–311 (2009).
37. Liu, M. et al. Investigating the shared genetic architecture between depression and subcortical volumes. *Nat. Commun.* **15**, 7647 (2024).
38. Dai, Y. et al. WebCSEA: web-based cell-type-specific enrichment analysis of genes. *Nucleic Acids Res.* **50**, W782–w790 (2022).
39. Li, M. et al. Integrative functional genomic analysis of human brain development and neuropsychiatric risks. *Science* <https://doi.org/10.1126/science.aat7615> (2018).
40. Akbarian, S. et al. The PsychENCODE project. *Nat. Neurosci.* **18**, 1707–1712 (2015).
41. Sakaue, S. & Okada, Y. GREP: genome for REPositioning drugs. *Bioinformatics* **35**, 3821–3823 (2019).
42. Wishart, D. S. et al. DrugBank 5.0: a major update to the DrugBank database for 2018. *Nucleic Acids Res.* **46**, D1074–d1082 (2018).
43. Seidlitz, J. et al. Morphometric similarity networks detect microscale cortical organization and predict inter-individual cognitive variation. *Neuron* **97**, 231–247 e237 (2018).
44. Griffith, M. et al. DGldb: mining the druggable genome. *Nat. Methods* **10**, 1209–1210 (2013).
45. Chen, W. et al. Melatonin improves the resistance of oxidative stress-induced cellular senescence in osteoporotic bone marrow mesenchymal stem cells. *Oxid. Med. Cell. Longev.* **2022**, 7420726 (2022).
46. Więdołcha, M. et al. Oxidative stress biomarkers among schizophrenia inpatients. *Brain Sci.* <https://doi.org/10.3390/brainsci13030490> (2023).
47. Correll, C. U. et al. Prevalence, incidence and mortality from cardiovascular disease in patients with pooled and specific severe mental illness: a large-scale meta-analysis of 3,211,768 patients and 113,383,368 controls. *World Psychiatry* **16**, 163–180 (2017).
48. Huang, E. J. & Reichardt, L. F. Trk receptors: roles in neuronal signal transduction. *Annu. Rev. Biochem.* **72**, 609–642 (2003).
49. Agarwal, R. et al. Pathogenesis of cardiomyopathy caused by variants in ALPK3, an essential pseudokinase in the cardiomyocyte nucleus and sarcomere. *Circulation* **146**, 1674–1693 (2022).
50. Biddinger, K. J. et al. Rare and common genetic variation underlying the risk of hypertrophic cardiomyopathy in a national biobank. *JAMA Cardiol.* **7**, 715–722 (2022).
51. Tseng, W. C. et al. Schizophrenia-associated SLC39A8 polymorphism is a loss-of-function allele altering glutamate receptor and innate immune signaling. *Transl. Psychiatry* **11**, 136 (2021).
52. Mealer, R. G. et al. The schizophrenia risk locus in SLC39A8 alters brain metal transport and plasma glycosylation. *Sci. Rep.* **10**, 13162 (2020).
53. Duarte, R. R. R. et al. Genome-wide significant schizophrenia risk variation on chromosome 10q24 is associated with altered cis-regulation of BORCS7, AS3MT, and NTS2C in the human brain. *Am. J. Med. Genet. B Neuropsychiatr. Genet.* **171**, 806–814 (2016).
54. Wu, X. L., Yan, Q. J. & Zhu, F. Abnormal synaptic plasticity and impaired cognition in schizophrenia. *World J. Psychiatry* **12**, 541–557 (2022).
55. Oliveras-Cañellas, N. et al. Adipose tissue coregulates cognitive function. *Sci. Adv.* **9**, eadg4017 (2023).
56. Sharkey, K. A. Integrative action of the autonomic nervous system: neurobiology of homeostasis. 2006. By Wilfrid Jänig. Published by Cambridge University Press. 610 pages. Price C\$200. *Can. J. Neurol. Sci.* **35**, 123–123 (2008).
57. Benarroch, E. What is the role of the sympathetic system in skeletal muscle? *Neurology* **102**, e209488 (2024).
58. Franzoso, M., Dokshokova, L., Vitiello, L., Zaglia, T. & Mongillo, M. Tuning the consonance of microscopic neuro-cardiac interactions allows the heart beats to play countless genres. *Front. Physiol.* **13**, 841740 (2022).
59. Benarroch, E. E. Physiology and pathophysiology of the autonomic nervous system. *Continuum* **26**, 12–24 (2020).
60. Furness, J. B. The enteric nervous system and neurogastroenterology. *Nat. Rev. Gastroenterol. Hepatol.* **9**, 286–294 (2012).
61. Lintunen, J., Lähteenvuuo, M., Tiitonen, J., Tanskanen, A. & Taipale, H. Adenosine modulators and calcium channel blockers as add-on treatment for schizophrenia. *NPJ Schizophr.* **7**, 1 (2021).
62. Wang, Z. et al. Pleiotropic association of CACNA1C variants with neuropsychiatric disorders. *Schizophr. Bull.* **49**, 1174–1184 (2023).
63. Refisch, A. et al. Analysis of CACNA1C and KCNH2 risk variants on cardiac autonomic function in patients with schizophrenia. *Genes* <https://doi.org/10.3390/genes13112132> (2022).
64. Howard, D. M. et al. Genome-wide meta-analysis of depression identifies 102 independent variants and highlights the importance of the prefrontal brain regions. *Nat. Neurosci.* **22**, 343–352 (2019).

65. Tan, J. et al. Progress in the application of molecular imaging in psychiatric disorders. *Psychoradiology* **3**, kkad020 (2023).

## ACKNOWLEDGEMENTS

Figure 1 was supported by the Figdraw platform (<https://www.figdraw.com/>) and the Servier Medical Art (<https://smart.servier.com/>), licensed under a Creative Commons Attribution 4.0 Unported License. This work was supported by Postdoctoral Research Start-up Fund of The First Affiliated Hospital of Fujian Medical University (BSH4281); Startup Fund for Scientific Research of Fujian Medical University (2024QH1082); Natural Science Foundation of Fujian Province (2025J08168).

## AUTHOR CONTRIBUTIONS

Dairong Cao and Yingying Xie designed the study. Yingying Xie and Jiaojiao Du analyzed the data. Yingying Xie and Jiaojiao Du wrote the manuscript. Feng Liu, Zhen Zhao, Jie Sun, Zhang Zhang, and Ningnannan Zhang supervised this work. All authors critically reviewed the manuscript.

## COMPETING INTERESTS

The authors declare no competing interests.

## ADDITIONAL INFORMATION

**Supplementary information** The online version contains supplementary material available at <https://doi.org/10.1038/s41537-025-00670-6>.

**Correspondence** and requests for materials should be addressed to Feng Liu or Dairong Cao.

**Reprints and permission information** is available at <http://www.nature.com/reprints>

**Publisher's note** Springer Nature remains neutral with regard to jurisdictional claims in published maps and institutional affiliations.



**Open Access** This article is licensed under a Creative Commons Attribution-NonCommercial-NoDerivatives 4.0 International License, which permits any non-commercial use, sharing, distribution and reproduction in any medium or format, as long as you give appropriate credit to the original author(s) and the source, provide a link to the Creative Commons licence, and indicate if you modified the licensed material. You do not have permission under this licence to share adapted material derived from this article or parts of it. The images or other third party material in this article are included in the article's Creative Commons licence, unless indicated otherwise in a credit line to the material. If material is not included in the article's Creative Commons licence and your intended use is not permitted by statutory regulation or exceeds the permitted use, you will need to obtain permission directly from the copyright holder. To view a copy of this licence, visit <http://creativecommons.org/licenses/by-nc-nd/4.0/>.

© The Author(s) 2025